JACS
JOURNAL OF THE AMERICAN CHEMICAL SOCIETY
Article
pubs.acs.org/JACS

Assembly-Induced Enhancement of Cu Nanoclusters Luminescence with Mechanochromic Property

Zhennan Wu,[†] Jiale Liu,[†] Yang Gao,[‡] Huiwen Liu,[†] Tingting Li,[†] Haoyang Zou,[†] Zhigang Wang,[‡] Kai Zhang,[†] Yue Wang,[†] Hao Zhang,*[,†] and Bai Yang[†]

[†]State Key Laboratory of Supramolecular Structure and Materials, College of Chemistry, Jilin University, Changchun 130012, PR China

[‡]Institute of Atomic and Molecular Physics, Jilin University, Changchun 130012, PR China

Supporting Information

ABSTRACT: Metal nanoclusters (NCs) as a new class of phosphors have attracted a great deal of interest owing to their unique electronic structure and subsequently molecule-like optical properties. However, limited successes have been achieved in producing the NCs with excellent luminescent performance. In this paper, we demonstrate the significant luminescence intensity enhancement of 1-dodecanethiol (DT)-capped Cu NCs via self-assembly strategy. By forming compact and ordered assemblies, the original nonluminescent Cu NCs exhibit strong emission. The flexibility of self-assembly allows to further control the polymorphism of Cu NCs assemblies, and hence the emission properties. Comparative structural and optical analysis of the polymorphic NCs assemblies permits to establish a relationship between the compactness of assemblies and the emission. First, high compactness reinforces the cuprophilic Cu(I)···Cu(I) interaction of inter- and intra-NCs, and meanwhile, suppresses intramolecular vibration and rotation of the capping ligand of DT, thus enhancing the emission intensity of Cu NCs. Second, as to the emission energy that depends on the distance of Cu(I)···Cu(I), the improved compactness increases average Cu(I)···Cu(I) distance by inducing additional inter-NCs cuprophilic interaction, and therewith leads to the blue shift of NCs emission. Attributing to the assembly mediated structural polymorphism, the NCs assemblies exhibit distinct mechanochromic and thermochromic luminescent properties. Metal NCs-based white light-emitting diodes are further fabricated by employing the NCs assemblies with blue-green, yellow, and red emissions as phosphors.

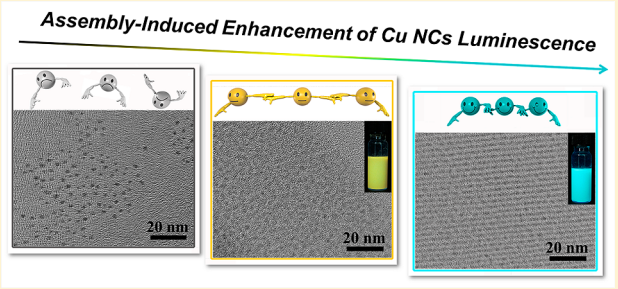

INTRODUCTION

Metal nanoclusters (NCs), consisting of a few to a hundred atoms, possess unique electronic structure, because their sizes are comparable to the Fermi wavelength of electrons.[1−6] They show molecule-like optical properties, and greatly inspire the recent research regarding them as novel fluorophores.[7−11] Metal NCs exhibit ultrafine size, low toxicity, good biocompatibility, and large Stokes shift, which make them appealing alternatives to organic dyes and semiconductor quantum dots in biosensing and bioimaging.[12−15] However, limited studies and breakthroughs have focused on broadening the applications concerning their phosphors nature, such as light-emitting diodes (LEDs). The reason mainly involves three aspects.[16−18] First, the small size usually induces aggregation and/or oxidation both in storage and further employment. Second, it still suffers from the limitation in convenient and universal preparation. Finally, the complex emission types together with a lacking acquaintance of luminescence mechanism lead to poor control of emission color and intensity.

With respect to the luminescence mechanism, the origin of NCs emission cannot be simply attributed to the quantum confinement effect of small metal core, but also relates to the capping ligands on NCs surface.[2,19−21] The coordination of metal core with ligands usually leads to ligand-to-metal charge transfer (LMCT) and/or ligand-to-metal−metal charge transfer (LMMCT), and therewith generates radiative relaxation via a metal-centered triplet state.[20] Because of the unclear surface or interfacial structure, it is still difficult to distinguish the contribution of metal core and capping ligands, especially for the larger NCs with complex surface structure.[2] Recently, the efforts on conducting NCs surface ligands configuration have been successfully applied for the luminescence enhancement by controlling NCs aggregation structures.[20,22,23] The aggregation of NCs is capable to alter the ligand/ligand, ligand/metal, and metal/metal interactions, which in return affects the excited state relaxation dynamics.[20] In particular, the intramolecular vibration and rotation of ligands are strongly restrained after aggregation, thus increasing the rates of radiative energy transfer by suppressing ligand-related nonradiative relaxation of excited states.[22,23] So far, solvent- and cation-induced aggregations are two major approaches for NCs luminescence enhancement.[20,22,23] However, both these two approaches meet the challenge of inhomogeneity of NCs aggregation structures,

Received: June 24, 2015
Published: September 23, 2015

DOI: 10.1021/jacs.5b06550
J. Am. Chem. Soc. 2015, 137, 12906−12913

which leads to the coexistence of inhomogeneous and multiple surface-ligands-determined chromophores in the system.[20] Consequently, such aggregation-induced enhancement only generates the fluorophores with low emission intensity, poor color-purity, and high unstability, thus restricting the potential applications.[20] Novel methods are greatly welcome to improve the emission performance of NCs aggregation structures by in depth revealing the mechanism of aggregation-induced enhancement.

Self-assembly has been regarded as an efficient strategy for optimizing the performance of nanometer-sized building blocks by directing their spatial distribution.[24−28] The alternation of NCs connection fashion greatly influences charge and energy transfer, and therefore the photoelectric performance.[29] As to the enhancement of NCs luminescence, self-assembly technique is considered to produce the architectures with inner NCs in ordered, uniform, and steady manner.[25,26] Thus, the homogeneity of NCs aggregation structures may be improved by forming regular self-assembly architectures. The transformation of disordered aggregates to ordered assemblies is hopeful for enhancing NCs luminescence performance, including intensity, color-purity, stability, and so forth. However, limited successes have been achieved in conducting the self-assembly of ultrasmall NCs into regular architectures.[30−32] As to NCs, their large surface energy prefers to induce irregular aggregation and fusion rather than form ordered and stable self-assembly structures. In particular, the thermal fluctuation energy of environment is comparable to the interactions between NCs, which usually detaches the assembled NCs and restricts the formation of ordering structures. Recently, on the basis of the exploration on the self-assembly kinetics of ligands-capped metal NCs, regular NCs self-assembly structures are obtained with controlled manner in the mixture of high-boiling-point solvents.[33,34] This success makes it possible for in depth studying the mechanism of NCs luminescence enhancement and producing highly luminescence NCs materials.

In this paper, 1-dodecanethiol (DT)-capped Cu NCs are prepared in colloidal solution and selected as the model to produce NCs aggregation structures with different regularity. By controlling the aggregation/assembly fashion as well as studying the mechano- and thermochromic luminescent properties, the dependence of NCs emission on the regularity of aggregation structures is well revealed. It indicates that the transformation of NCs architectures from disordered aggregates to ordered assemblies is capable to generate strong emission. This is attributed to the improved interactions of DT on neighboring NCs, which suppress DT-related nonradiative relaxation of excited states and subsequently optimize the radiative energy transfer on the basis of LMCT and/or LMMCT. With respect to the self-assembly architectures, the improved compactness increases the average distance of cuprophilic Cu(I)···Cu(I) by inducing additional inter-NCs cuprophilic interaction, and therewith leads to the blue shift of emission. Because of the assembly induced enhancement, the NCs assemblies are further applied as phosphors in fabricating LEDs. A white LED (WLED) prototype is demonstrated by employing the NCs assemblies as color conversion layer on 365 nm GaN LED chip.

EXPERIMENTAL SECTION

Chemicals. 1-Dodecanethiol (DT, 98%) was purchased from Aladdin Chemistry Co. Ltd.. Dibenzyl ether (BE, 98%), and polydimethylsiloxane (PDMS) precursors were purchased from Aldrich. Copper chloride ($CuCl_2{\cdot}2H_2O$, 99.0%, A. R.), chloroauric acid ($HAuCl_4{\cdot}4H_2O$, Au mol % > 47.8%), acetone, and chloroform were all commercially available products and used as received without further purification.

Preparation of Cu NCs. Thirty mg (0.18 mmol) of $CuCl_2{\cdot}2H_2O$ was dissolved in 6 mL of BE at room temperature with the assistance of ultrasonic treatment for 10 min. One mL (4 mmol) of DT, which acted as ligand *cum* reductant, was added into the mixture and stirred at 0 °C for 5 min to produce DT-capped Cu NCs.

Self-Assembled Cu NCs. To assemble Cu NCs into ribbons, 30 mg (0.18 mmol) of $CuCl_2{\cdot}2H_2O$ was dissolved in 6 mL of BE at room temperature with ultrasonic treatment for 10 min. Then, 1 mL (4 mmol) of DT was added into the mixture and stirred at 128 °C for 3 h. The preparation of self-assembled sheets of Cu NCs was similar to that of ribbons, except annealing the reaction mixture to 20 °C and maintaining for 24 h.

Self-Assembled Au NCs. 0.2 g (0.48 mmol) of $HAuCl_4{\cdot}4H_2O$ was dissolved in 10 mL of BE at room temperature with ultrasonic treatment for 10 min. Then, 0.5 mL (2 mmol) of DT was added into the mixture and stirred at 140 °C for 1 h. The products were self-assembled sheets from Au NCs.

Purification. At room temperature, 1 mL of Cu NCs solution or the self-assembled Cu NCs ribbons/sheets, and Au NCs sheets were washed and precipitated through the addition of 2 mL of chloroform and 4 mL of acetone for two times. Separated by centrifugation, the precipitates were collected and dispersed in 1 mL of chloroform. After purification, the yield of Cu NCs, Cu NCs self-assembly ribbons, Cu NCs self-assembly sheets, and Au NCs self-assembly sheets was ∼95%, ∼81%, ∼98%, and ∼85%, respectively. In solution or as solid powder, these samples can be stored in air at least for one year without obvious structural and luminescence variation.

Fabrication of LEDs from As-Assembled Cu and/or Au NCs. GaN LED chips without phosphor coating were purchased from Advanced Optoelectronic Technology CO., Ltd. The emission of the GaN LED chip centered at 365 nm, and the operating voltage was 4.0 V. In the preparation of color conversion layer, Cu and/or Au NCs assemblies with different emission colors were foremost mixed with specific ratio and milled to fine powder. Then, the PDMS precursors were mixed with the powder with the ratio of 15:5 (w/w). The mixtures were put into a vacuum chamber to remove bubbles. After that, the mixtures were loaded on the LED chip. After curing at 60 °C for 2 h, the LEDs from as-assembled Cu and/or Au NCs were fabricated.

Characterization. UV−visible absorption spectra were obtained using a Shimadzu 3100 UV−vis spectrophotometer. Fluorescence spectroscopy was performed with a Shimadzu RF-5301 PC spectrophotometer. The absolute quantum yield (QY) of NCs was measured on Edinburgh FLS920 (excited at 365 nm) equipped with an integrating sphere. The luminescence decay curves were measured on a FLS920 spectrofluorometer. Transmission electron microscopy (TEM) was conducted by a Hitachi H-800 electron microscope. High-resolution TEM (HRTEM) images were implemented by a JEM-2100F electron microscope. An energy-dispersive X-ray spectroscopy (EDX) detector coupled with HRTEM was applied for elemental analysis. Small-angle X-ray powder diffraction (SXRD) investigation was carried out on a Rigaku X-ray diffractometer using Cu K radiation (λ = 1.54 Å). X-ray photoelectron spectroscopy (XPS) was investigated with a VG ESCALAB MKII spectrometer. Thermo gravimetric analysis (TGA) was measured on an American TA Q500 analyzer under N2 atm with the flow rate of 70 mL/min. Matrix-assisted laser desorption/ionization time-off light (MALDI-TOF) mass spectra (MS) were recorded on a Bruker/Auto Reflex III mass spectrometer equipped (Bremen, Germany), where THF and 2,5-dihydroxybenzoic acid (DHBA) were used as the matrix to dissolve the samples. Scanning electron microscope (SEM) image was taken by a JEOL FESEM 6700F electron microscope with primary electron energy of 3 kV. Atomic force microscope (AFM) tapping mode measurements were performed with a Nanoscope IIIa scanning probe microscope (Digital Instruments) using a rotated tapping mode etched

DOI: 10.1021/jacs.5b06550
J. Am. Chem. Soc. 2015, 137, 12906−12913

silicon probe tip. The spectra of the LEDs were measured under ambient condition at room temperature by combining a Spectrascan PR-650 spectrophotometer with an integrating sphere and a computer-controlled direct-current power. The color of the light was identified by the CIE (Commission Internationale de L'Eclairage 1931) calorimeter system.

RESULTS AND DISCUSSION

Individual Cu NCs without Visible Emission. The Cu NCs employed to investigate assembly induced luminescence enhancement are foremost synthesized in BE using DT as ligand *cum* reductant at 0 °C. TEM observation indicates that the as-prepared NCs appear as quasi-spherical clusters with the average diameter of 1.9 ± 0.2 nm (Figure 1a). By combining

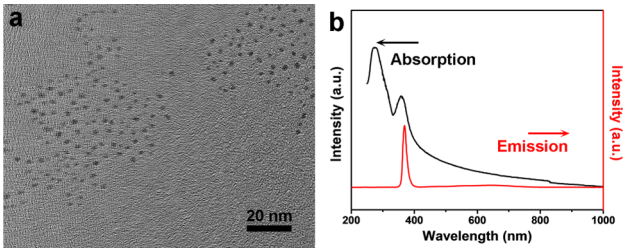

Figure 1. (a) TEM image of individual Cu NCs. (b) Steady-state absorption (black) and emission (red) spectra of Cu NCs in chloroform. The peak in red line results from the excitation light source of 365 nm.

EDX, MALDI-TOF MS, TGA, and XPS measurements, the composition of NCs is suggested as $Cu(0)_4Cu(I)_{10}DT_{10}$ (Figure S1–S4). The UV–vis absorption spectrum of the NCs exhibits two peaks respectively at 275 and 358 nm (Figure 1b). The simulated absorption spectrum by time-dependent density functional theory indicates that the excited states with relatively strong oscillator strength consist well with the experimentally measured values ranging from 250 to 400 nm. The two absorption peaks originate from the transition of S–Cu hybrid bonding orbital to Cu–Cu hybrid bonding orbital (Figure S5), namely, the transition between occupied 3p-4s3d hybrid orbital and unoccupied 4s4p hybrid orbital. This confirms the suggested formula of $Cu(0)_4Cu(I)_{10}DT_{10}$ (Figure 1b and Figure S5). No visible emission is observed by 365 nm excitation, showing the poor emission of individual Cu NCs (Figure 1b). However, weak orange emission is observed after acetone-induced aggregation, which also presents excitation dependence (Figure S6a–c).

Emission Intensity Increase by Cu NCs Self-Assembly. The self-assembly of Cu NCs into ribbons is performed by annealing NCs BE solution at 128 °C for 3 h. The annealing treatment facilitates the dynamic mobility of DT alkyl chain on NCs, thus permitting the two-dimensional oriented self-assembly of NCs via dipole-induced asymmetric van der Waals attraction.[36] Note that the occurrence of self-assembly is the characteristics of nanometer-sized metal clusters, which is independent of the species of metal. However, the morphology of self-assembly architectures greatly depends on the species of metal by influencing the coordination of various inter-NCs weak interactions.[36] Cu generates strong inter-NCs dipolar attraction.[33] So, Cu NCs prefer to form self-assembly ribbons with one-dimensional orientation. The ribbons indicate the average width about 50–200 nm, length about 1–2 um, and thickness about 13.5 nm (Figure 2a, S7 and S8). Because of the

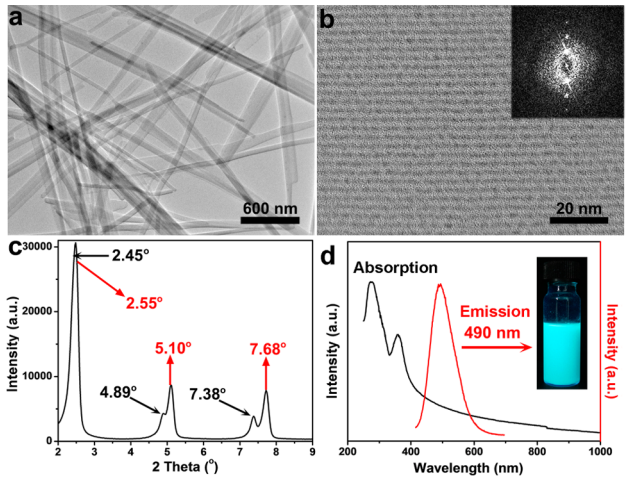

Figure 2. (a) TEM image of the ribbons from Cu NCs self-assembly. (b) HRTEM image of the ribbons. Inset: the Fourier transform image. (c) Small-angle region of XRD pattern. (d) Steady-state absorption (black) and emission (red) spectra of the ribbons in chloroform. Inset: the fluorescent image with 365 nm excitation.

high surface energy, the ribbons are easy to form parallel array or show twisted and bent structures (Figure 2a). TEM images reveal that the ribbons are composed of individual NCs rather than crystalline Cu (Figure 2b and S9a). Within the ribbons, the Cu NCs exhibits highly ordered arrangement, which is further proved by the intense peaks in SXRD (Figure 2b,c). There are two distinct diffraction peaks at 2.45 and 2.55°, which correspond to the *d* spacing of 3.6 and 3.4 nm. The second and third ordered peaks are also observed at 4.89–5.10° and 7.38–7.68°. As to the ribbons, they are stacked from the self-assembly monolayer of NCs.[34] There exist two different NCs center-to-center distances, namely intra- and interlayer NC distance.[34] The former is larger than the latter.[36] So, the *d* spacing of 3.6 nm relates to the alignment of Cu NCs within self-assembly monolayer, whereas the *d* spacing of 3.4 nm corresponds to the NC distance between the neighboring layers. It should be mentioned that the size and composition of NCs are fixed at 1.9 ± 0.2 nm and $Cu_{14}DT_{10}$, respectively, before and after self-assembly (Figure 1a, 2b, S1, S2, S4 and S9a), showing no growth and fusion of NCs during self-assembly. This consideration is also supported by the unchanged absorption spectra (Figure 1b and 2d).

Despite the size, composition, structure, and absorption property of Cu NCs are unchanged, a dramatic intensity increase of NC emission is found after self-assembly (Figure 2d). The NCs assemblies exhibit a strong emission peak centered at 490 nm with a full width at half-maximum (fwhm) around 86 nm, corresponding to blue-green emission (Figure 2d). The absolute QY of the assemblies is measured up to 6.5%, which is among the highest values of ever reported Cu NCs.[11,21,35] The PL decay at 490 nm is described with a two-exponential fitting. The average lifetime is calculated as 1.76 μs by integrating two individual lifetimes of 0.77 μs (55.7%) and 3.02 μs (44.3%) (Figure S10). Combining with the long excited-state lifetime with large Stokes shift (>200 nm), the emission intensity increase after Cu NCs self-assembly should relate to the coordination of metal core with the capping ligand of DT, namely the charge transfer through LMCT and/or LMMCT.[20] This generates radiative relaxation via a metal-centered triplet state.[19] In this situation, during the trans-

DOI: 10.1021/jacs.5b06550
J. Am. Chem. Soc. 2015, 137, 12906–12913

formation of NCs aggregation structures from disordered aggregates to ordered assemblies, the subtle variation of NCs mainly involves the DT interactions on NCs surface and the cuprophilic Cu(I)···Cu(I) interaction.[37] Thus, the assembly induced emission enhancement is assigned to two aspects. First, the enhanced inter- and intra-NCs cuprophilic interactions greatly facilitate the excited state relaxation dynamics via radiative pathway.[38,39] Second, the restriction of intramolecular vibration and rotation of capping ligands reduces the nonradiative relaxation of excited states.[20,40−42] These two effects greatly enhance the emission intensity of NCs after self-assembly.

To further illuminate the self-assembly induced emission intensity increase, self-assembled sheets of Cu NCs with loose aggregation structures are fabricated (Figure 3a). After self-assembly, the size and composition of Cu NCs are also unchanged (Figure S1, S2, S4 and S9b). The sheets indicate the average width about 200−800 nm, length about 0.4−2 um, and thickness about 2.1 nm (Figure 3a, S11 and S12). In comparison to the ribbons, the formation of sheets is performed at lower annealing temperature of 20 °C but longer duration of 24 h. Low temperature suppresses the mobility of DT alkyl chains, and hence the winding of DT on neighboring NCs.[33,34,36] This decreases the DT interaction and results in the loose assembly structures. TEM image reveals the loose arrangement of NCs in the sheets (Figure 3b), which consists with the SXRD result (Figure 3c). Only one weak diffraction peak appears at 2.46°, while the second and third ordered peaks locate at 5.07° and 7.66°. Because of the loose arrangement of inner NCs, the sheets exhibit lowered QY of 3.6%. This result confirms that the emission intensity strongly depends on the compactness of NCs assemblies. The loose assembly weakens the inter-NCs cuprophilic interaction. Meanwhile, it becomes less capable to restrict intramolecular vibration and rotation of capping ligands, and therefore the nonradiative relaxation of excited states.

Notably, in parallel to emission intensity decreases, the formation of sheets with low compact NCs arrangement leads to a redshift of emission spectrum to 547 nm with a fwhm around 84 nm (Figure 3d). The apparent emission color turns yellow. By combining MALDI-TOF MS, EDX, XPS, and TEM characterizations, the size effect on the spectral red shift is safely excluded, because the size and composition of NCs are unchanged (Figure S1, S2, S4 and S9). So, the shift of emission spectrum is attributed to the alteration of average Cu(I)···Cu(I) distance.[37] In this context, the increase of Cu(I)···Cu(I) distance leads to the blue shift of luminescence, while distance decrease causes red shift. There exist two kinds of cuprophilic interactions that influence the average Cu(I)···Cu(I) distance and hence the emission color. One is the intrinsic cuprophilic interaction within Cu NCs. Another is the cuprophilic interaction between the neighboring NCs, which possesses longer distance feature and is generated only after forming compact NCs self-assembly architectures. The improved compactness of Cu NCs from individual NCs to self-assembly ribbons induces additional inter-NCs cuprophilic interaction, thus increasing the average Cu(I)···Cu(I) distance. As a result, blue-green emission is generated. As to the sheets with loose NCs arrangement, the inter-NCs cuprophilic interaction is weaker than that of ribbons. The effect on the average Cu(I)···Cu(I) distance is not obvious. So, as the self-assembly structures transform from ribbons to sheets, the average Cu(I)···Cu(I) distance is shortened, which leads to the decrease of emission energy and spectral red shift. This is different from the previous reports about metal organic complexes, which do not present the correlation between metal−metal interaction and luminescence properties.[43] In addition, due to the dipole-induced asymmetric van der Waals attraction, the surface ligands of NCs redistribute during NCs self-assembly,[36] thus overcoming the steric hindrance of the ligands and permitting the occurrence of inter-NCs cuprophilic interaction. Under TEM, the distance of a lot of NCs are really very close (Figure S9).

The annealing temperature-dependent compactness of Cu NCs self-assembly is applied to control the emission color and intensity of the as-prepared assemblies (Figure 4). As increasing the annealing temperature from 20 to 120 °C, the apparent emission turns from yellow to blue-green, accompanying with the enhancement of emission intensity, despite the absorption spectra are unchanged. According to the aforementioned explanation, lower annealing temperature is considered to produce looser assemblies. The weak winding between the DT on NCs surface is difficult to restrict the molecular vibration and rotation of DT, thus increasing the ratio of nonradiative relaxation of excited states. This lowers the emission intensity. In addition, the dominant intra-NCs cuprophilic interaction shortens the overall Cu(I)···Cu(I) distance, and therewith leads to lower emission energy. In contrast, higher temperature

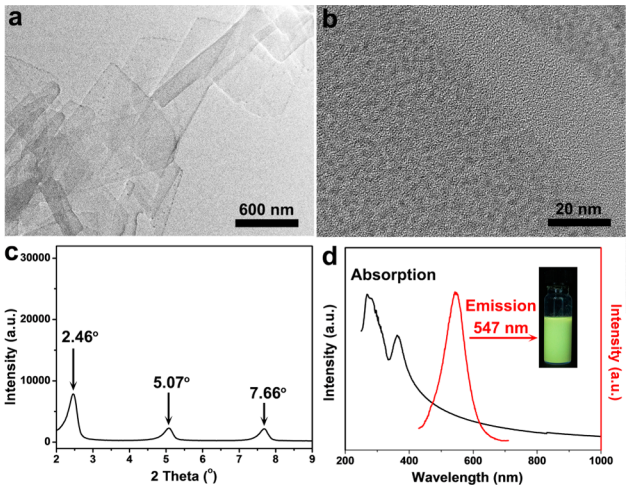

Figure 3. (a) TEM image of the sheets from Cu NCs self-assembly. (b) HRTEM image of the sheets. (c) Small-angle region of XRD pattern. (d) Steady-state absorption (black) and emission (red) spectra of the sheets in chloroform. Inset: the fluorescent image with 365 nm excitation.

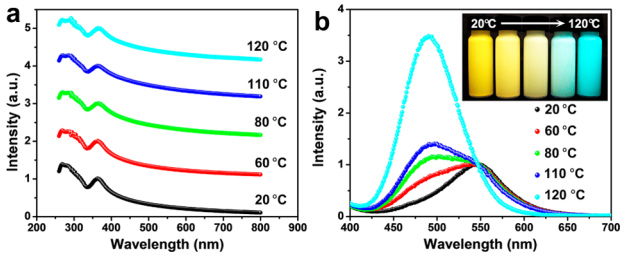

Figure 4. Steady-state absorption (a) and emission (b) spectra of Cu NCs assemblies respectively prepared at 20, 60, 80, 110, and 120 °C. Inset: the fluorescent images with 365 nm excitation.

DOI: 10.1021/jacs.5b06550
J. Am. Chem. Soc. 2015, 137, 12906−12913

facilitates the formation of compact assemblies, and enhances the emission intensity with spectral blue shift. Polymorphism change of NCs assemblies is the main reason for influencing the emission performance.

Mechano- and Thermochromic Luminescence of Cu NCs Assemblies. The relationship between the compactness of NCs assemblies and their emission properties is further revealed by studying the mechanochromic luminescence of as-assembled ribbons and sheets. As shown in Figure 5, the as-

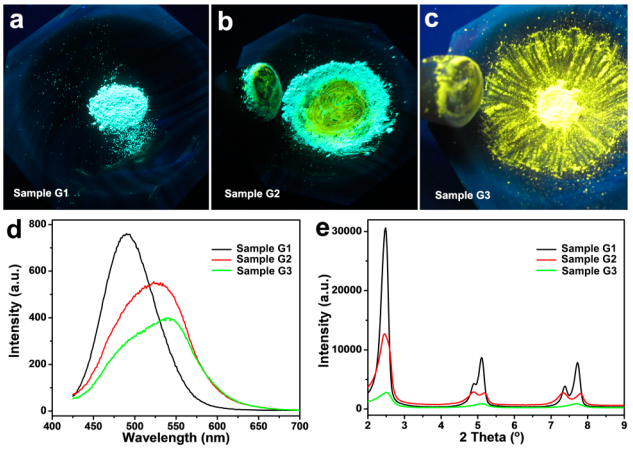

Figure 5. Fluorescent images of sample G1 (a), G2 (b), and G3 (c) with 365 nm excitation. (d) Emission spectra of the three samples in chloroform with 365 nm excitation. (e) SXRD patterns of the three samples.

assembled ribbons exhibit mechanochromic luminescence, which is often observed in organic and organometallic complexes.[44−51] The ribbons without grinding, with partially grinding, and thoroughly grinding are labeled as sample G1, G2, and G3. The grinding treatment does not alter the composition of Cu NCs, but leads to a dramatic change both in the emission color and intensity (Figure S13 and 5a−d). Accompanied with the variation of emission color from blue-green to yellow, the QY decreases from 6.5% to 3.8%. The fwhm also increases from 106 to 111 nm (Figure 5d). In addition, the spectral shift involves the decrease of 490 nm emission and the appearance of 547 nm emission, implying the transformation of NCs assemblies from order to disorder.

This consideration is proved by TEM observation and SXRD results (Figure 5e and S14). After grinding, the thickness and regularity of the self-assembly ribbons decrease (Figure S14). SXRD patterns exhibit the intensity decrease and broadening of diffraction peaks after grinding. The original two sets of diffraction peaks alter to one set. These reveal the decreased regularity of NCs in the assemblies (Figure 5e). Moreover, the self-assembly sheets, which possess intrinsic loose NCs arrangement, do not exhibit obvious emission change after grinding (Figure S15). This result confirms that grinding treatment only disarrange the compactness of NCs in regular assemblies, thus altering DT and/or NCs interactions, whereas the NCs self-assembly architectures are not completely destroyed. It also indicates the good stability of NCs emission.

The presence of polymorphism of Cu NCs assemblies also leads to structure-dependent thermochromic luminescence (Figure 6). Despite the fact that the emission of ribbons and sheets at room temperature is quite different, such difference becomes less as dipping the samples in liquid nitrogen (77 K)

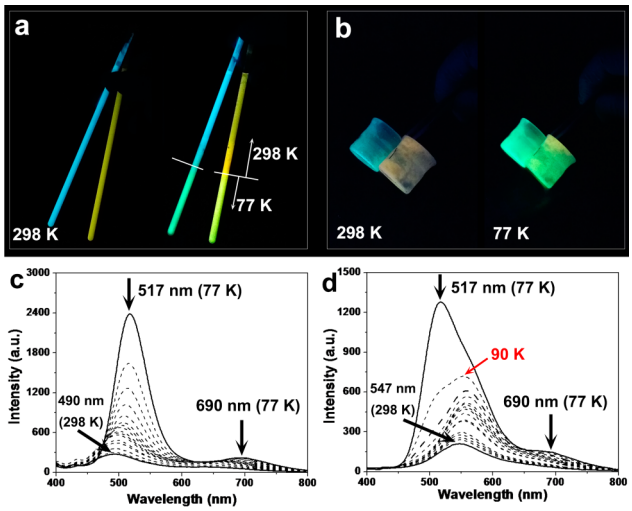

Figure 6. Fluorescent images of the solution (a) and powder (b) of Cu NCs self-assembly ribbons and sheets with 365 nm excitation at 298 and 77 K. The variation of emission spectra of ribbons (c) and sheets (d) with 365 nm excitation from 77 to 298 K.

(Figure 6a,b). With 365 nm excitation, the original blue-green emission of ribbons centered at 490 nm shifts to 517 nm, showing the emission color of bright green (Figure 6c). Whereas, the yellow emission of sheets centered at 547 nm also shifts to 517 nm (Figure 6d). Notably, as lowering the temperature, a new emission band appears at 690 nm both for ribbons and sheets (Figure 6c,d). It is assigned to "ligand-centered" excited state,[37] which is independent of the nature of metal-cores but extremely sensitive to the surroundings and temperature. In addition, both the ribbons and sheets exhibit emission intensity increase at 77 K. The QY of ribbons is up to 20%. Such thermochromic luminescence is reversible as cycling the temperature from 77 to 298 K. The intensity increase at 77 K can be comprehended according to the temperature-dependent interactions between NCs and DT in the assemblies. At low temperature, both inter- and intra-NCs cuprophilic interactions are reinforced. In particular, the intramolecular vibration and rotation of DT are greatly restricted. These favor radiative relaxation of excited states, thus leading to strong emission.

The temperature-dependent emission shift is much complex. In general, the emission of ribbons exhibits red shift at low temperature, while the emission of sheets shows blue shift. However, the emission of sheets first shows red shift until 90 K, and then blue shift occurs (Figure 6d). Because the emission energy is an external expression of overall Cu(I)···Cu(I) distance, the emission shift can be employed to determine the inner structural variation of NCs assemblies. In this context, the overall Cu(I)···Cu(I) distance relates to inter-NCs and intra-NCs distances. As to the ribbons, the decreased temperature both shortens inter-NCs and intra-NCs Cu(I)···Cu(I) distances, because NCs are limited in compact assemblies. Consequently, the emission continuously red shifts (Figure 6c). For the sheets, the variation of Cu(I)···Cu(I) distance at the initial stage of temperature decrease is similar. However, owing to the noncompact connection of neighboring NCs, further lowering temperature decreases intra-NCs Cu(I)···Cu(I) distance but increase inter-NCs Cu(I)···Cu(I) distance. When the increase in inter-NCs Cu(I)···Cu(I) distance becomes dominant, the blue shift of emission is inevitable

DOI: 10.1021/jacs.5b06550
J. Am. Chem. Soc. 2015, 137, 12906−12913

(Figure 6d). This consideration is also supported by the spectral variation as freezing acetone-induced Cu NCs aggregates at 77 K (Figure S6d,e). A significant blue shift of emission spectra is observed.

The structural disparity of ribbons and sheets is also reflected by the thermosensitivity. The thermosensitivity is nonlinear in the temperature range from 77 to 298 K, because of the mutable cuprophilic interactions. So, the thermosensitivity between 0 and 60 °C is revealed, which are 0.1 nm/°C for the ribbons and 0.15 nm/°C for the sheets (Figure 7a,b). Such

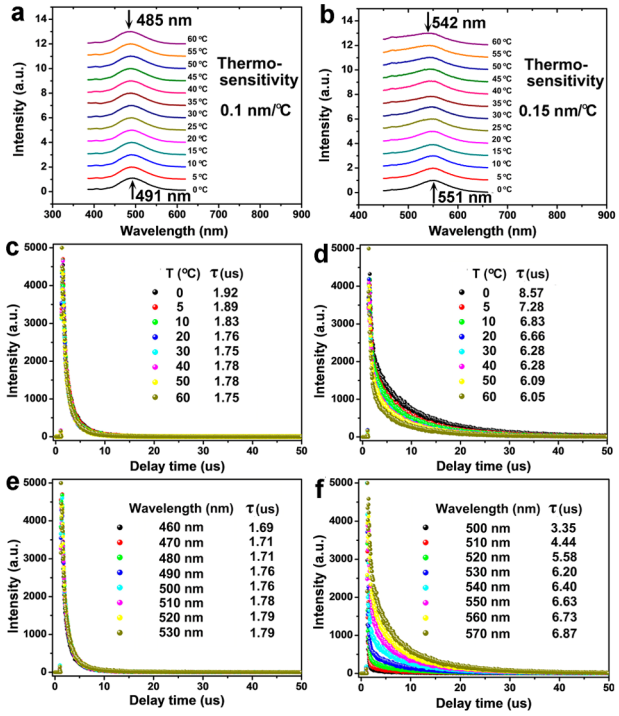

Figure 7. Temperature-dependent emission spectra of the ribbons (a) and sheets (b). Temperature-dependent luminescence lifetimes of the ribbons at 490 nm (c), and the sheets at 547 nm (d). (e) Luminescence lifetimes of the ribbons at 460, 470, 480, 490, 500, 510, 520, and 530 nm. (f) Luminescence lifetime of the sheets at 510, 520, 530, 540, 550, 560, and 570 nm. In all experiments, 365 nm excitation is adopted.

disparity is attributed to the different excited state relaxation dynamics of ribbons and sheets. This consideration is supported by studying the luminescence lifetime from 0 to 60 °C (Figure 7c,d). The average lifetime of ribbons is almost a constant about 1.83 ± 0.1 μs at 490 nm with 365 nm excitation. While the lifetime of sheets indicates monotonous decline from 8.57 to 6.05 μs at 547 nm. These results mean that ribbons possess homogeneous molecule-like chromophores on the basis of LMCT and/or LMMCT mechanism. To confirm whether sheets possess homogeneous chromophores, the steady- and transient-state emission of ribbons and sheets are explored (Figure S16). The emission peak position of both ribbons and sheets is independent of the excitation wavelength. This reveals that both ribbons and sheets possess homogeneous chromophores, namely, sole triplet state T1 (Figure 8).[52,53] Furthermore, as to the ribbons, the average lifetime almost keeps constant as altering the detection wavelength from 460 to 530 nm (Figure 7e), while the average lifetime of sheets gets longer with increasing the wavelength from 500 to 570 nm

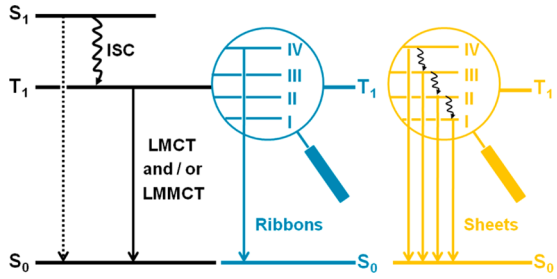

Figure 8. Energy level of ribbons and sheets, where S_0, T_1, and S_1 represent ground state, excited triplet state, and singlet state. I, II, III, and IV represent the sublevels of T1. ISC represents the intersystem crossing process.

(Figure 7f). This proves the existence of a series of electron trapping in the recombination process of sheets emission state.[42] Namely, the excited state relaxation dynamics in the T1 of sheets is more complex than that of ribbons (Figure 8). Unlike ribbons, the sheets possess low compactness of the composed NCs. The intramolecular vibration and rotation of ligands are also dynamic. These lead to relatively high ratio of ligand-related nonradiative relaxation between the sublevels of T1 excited states (Figure 8). As a result, the luminescence lifetime of sheets is longer than that of ribbons.

LEDs from Cu and Au NCs Assemblies. Because of the strong and tunable emission, the NCs assemblies are further employed as the color conversion layer for fabricating LEDs. In details, the LEDs are fabricated by mixing Cu NCs ribbons or sheets with PDMS precursors, depositing on commercially available GaN LED chip with the emission centered at 365 nm (Figure S17), and curing in an oven at 60 °C for 2 h. The LED devices with blue-green and yellow emissions are respectively fabricated using the self-assembly ribbons and sheets (Figure 9a,b,f,g). To demonstrate that WLEDs can be fabricated only from the combination of metal NCs, Au NCs sheets with similar NCs self-assembly structure of Cu NCs are chosen as the red emitting phosphors (Figure 9c,h and S18). In producing WLEDs, the Cu NCs ribbons with blue-green emission, Cu NCs sheets with yellow emission, and Au NCs sheets with red emission are mixed with specific ratio, and PDMS is employed as the media. A WLED prototype with color coordinate at (0.32, 0.36) is fabricated by combining Cu ribbons, Cu sheets, and Au sheets with the feed ratio of 1.2/1/1.5 (Figure 9d,e,i. To our best knowledge, it is the first example that employs metal NCs to produce WLEDs.

■ CONCLUSION

In summary, we demonstrate the enhancement of Cu NCs luminescence by forming compact and ordered self-assembly architectures. Such strategy reinforces the cuprophilic interaction of NCs, and suppresses intramolecular vibration and rotation of the capping ligands, thus greatly improving the radiative relaxation of excited states. Self-assembly strategy also permits to tune the regularity of NCs in the assemblies, which produces polymorphic Cu NCs assemblies with various emission colors. The transformation of polymorphism leads to mechanochromic luminescence of NCs assemblies. Because the NCs assemblies exhibit strong emission, they are employed as the phosphors in color conversion layer for fabricating LEDs. A WLED prototype is fabricated by combining the blue-green and yellow emission of Cu NCs assemblies and red emission of Au NCs assemblies. The current efforts perform an important

DOI: 10.1021/jacs.5b06550
J. Am. Chem. Soc. 2015, 137, 12906−12913

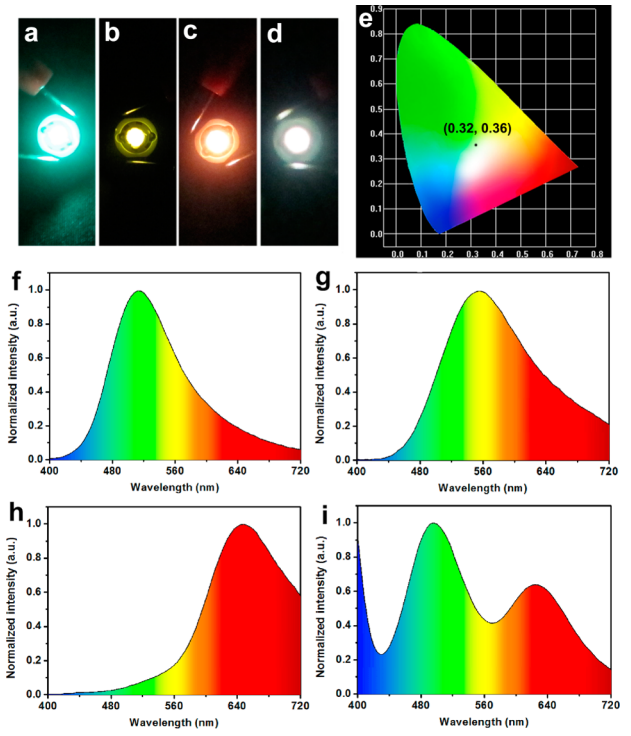

Figure 9. Fluorescent images of the LEDs from Cu NCs self-assembly ribbons (a), sheets (b), and Au NCs sheets (c). (d) Fluorescent image of the WLED from Cu NCs ribbons, Cu NCs sheets, and Au NCs sheets. (e) The CIE chromaticity coordinates of the WLED in (d). The corresponding emission spectra are shown in (f), (g), (h), and (i).

step toward further design and preparation of highly luminescent Cu NCs materials with controlled emission color and good stability, which greatly extends the potential of luminescent NCs in practical applications.

■ ASSOCIATED CONTENT

Supporting Information

The Supporting Information is available free of charge on the ACS Publications website at DOI: 10.1021/jacs.5b06550.

Additional characterizations of individual Cu NCs, Cu NCs assemblies, Cu NCs assemblies after grinding, DFT calculation, excitation dependence of Cu NCs assemblies, emission spectrum of GaN chip, and the characterizations of Au NCs assemblies. (PDF)

■ AUTHOR INFORMATION

Corresponding Author

*hao_zhang@jlu.edu.cn

Notes

The authors declare no competing financial interest.

■ ACKNOWLEDGMENTS

This work was supported by the 973 Program of China (2014CB643503), NSFC (51425303, 21374042, 21174051, 91123031, 21221063), and the Special Project from MOST of China.

■ REFERENCES

(1) Luo, Z.; Nachammai, V.; Zhang, B.; Yan, N.; Leong, D. T.; Jiang, D. E.; Xie, J. *J. Am. Chem. Soc.* **2014**, *136*, 10577.
(2) Chen, Y.; Yang, T.; Pan, H.; Yuan, Y.; Chen, L.; Liu, M.; Zhang, K.; Zhang, S.; Wu, P.; Xu, J. *J. Am. Chem. Soc.* **2014**, *136*, 1686.
(3) Qian, H.; Zhu, M.; Wu, Z.; Jin, R. *Acc. Chem. Res.* **2012**, *45*, 1470.
(4) Zhang, L.; Wang, E. *Nano Today* **2014**, *9*, 132.
(5) Yu, P.; Wen, X.; Toh, Y. R.; Ma, X.; Tang, J. *Part. Part. Syst. Charact.* **2015**, *32*, 142.
(6) Díez, I.; Ras, R. H. A. *Nanoscale* **2011**, *3*, 1963.
(7) Yan, Z.; Chen, Y. C.; Li, H. W.; Chang, H. T. *Chem. Commun.* **2014**, *50*, 9800.
(8) Yuan, X.; Luo, Z.; Zhang, Q.; Zheng, Y.; Lee, J. Y.; Xie, J. *ACS Nano* **2011**, *5*, 8800.
(9) Yu, Y.; Li, J.; Chen, T.; Tan, Y. N.; Xie, J. *J. Phys. Chem. C* **2015**, *119*, 10910.
(10) Wu, Z.; Lanni, E.; Chen, W.; Bier, M. E.; Ly, D.; Jin, R. *J. Am. Chem. Soc.* **2009**, *131*, 16672.
(11) Kawasaki, H.; Kosaka, Y.; Myoujin, Y.; Narushima, T.; Yonezawa, T.; Arakawa, R. *Chem. Commun.* **2011**, *47*, 7740.
(12) Yoshimoto, J.; Sangsuwan, A.; Osaka, I.; Yamashita, K.; Iwasaki, Y.; Inada, M.; Arakawa, R.; Kawasaki, H. *J. Phys. Chem. C* **2015**, *119*, 14319.
(13) Hofmann, C. M.; Essner, J. B.; Baker, G. A.; Baker, S. N. *Nanoscale* **2014**, *6*, 5425.
(14) Udayabhaskararao, T.; Pradeep, T. *J. Phys. Chem. Lett.* **2013**, *4*, 1553.
(15) Enkin, N.; Wang, F.; Sharon, E.; Albada, H. B.; Willner, I. *ACS Nano* **2014**, *8*, 11666.
(16) Yin, H.; Tang, H.; Wang, D.; Gao, Y.; Tang, Z. *ACS Nano* **2012**, *6*, 8288.
(17) Xie, J.; Zheng, Y.; Ying, J. Y. *J. Am. Chem. Soc.* **2009**, *131*, 888.
(18) Zheng, J.; Petty, J. T.; Dickson, R. M. *J. Am. Chem. Soc.* **2003**, *125*, 7780.
(19) Wu, Z.; Jin, R. *Nano Lett.* **2010**, *10*, 2568.
(20) Luo, Z.; Yuan, X.; Yu, Y.; Zhang, Q.; Leong, D. T.; Lee, J. Y.; Xie, J. *J. Am. Chem. Soc.* **2012**, *134*, 16662.
(21) Lin, Y. J.; Chen, P. C.; Yuan, Z.; Ma, J. Y.; Chang, H. T. *Chem. Commun.* **2015**, *51*, 11983.
(22) Liang, J.; Chen, Z.; Yin, J.; Yu, G. A.; Liu, S. H. *Chem. Commun.* **2013**, *49*, 3567.
(23) Jia, X.; Li, J.; Wang, E. *Small* **2013**, *9*, 3873.
(24) Si, K. J.; Sikdar, D.; Chen, Y.; Eftekhari, F.; Xu, Z.; Tang, Y.; Xiong, W.; Guo, P.; Zhang, S.; Lu, Y.; Bao, Q.; Zhu, W.; Premaratne, M.; Cheng, W. *ACS Nano* **2014**, *8*, 11086.
(25) Tang, Z.; Zhang, Z.; Wang, Y.; Glotzer, S. C.; Kotov, N. A. *Science* **2006**, *314*, 274.
(26) Xia, Y.; Nguyen, T. D.; Yang, M.; Lee, B.; Santos, A.; Podsiadlo, P.; Tang, Z.; Glotzer, S. C.; Kotov, N. A. *Nat. Nanotechnol.* **2011**, *6*, 580.
(27) Hong, X.; Tan, C.; Liu, J.; Yang, J.; Wu, X.-J.; Fan, Z.; Luo, Z.; Chen, J.; Zhang, X.; Chen, B.; Zhang, H. *J. Am. Chem. Soc.* **2015**, *137*, 1444.
(28) Tan, C.; Qi, X.; Liu, Z.; Zhao, F.; Li, H.; Huang, X.; Shi, L.; Zheng, B.; Zhang, X.; Xie, L.; Tang, Z.; Huang, W.; Zhang, H. *J. Am. Chem. Soc.* **2015**, *137*, 1565.
(29) Ni, W. X.; Qiu, Y. M.; Li, M.; Zheng, J.; Sun, R. W.; Zhan, S. Z.; Ng, S. W.; Li, D. *J. Am. Chem. Soc.* **2014**, *136*, 9532.
(30) Zhou, Y.; Zeng, H. C. *J. Am. Chem. Soc.* **2014**, *136*, 13805.
(31) Li, L.; Wang, Q. *ACS Nano* **2013**, *7*, 3053.
(32) Wang, F.; Zhang, X.; Zhang, Z.; He, C. *J. Mater. Chem.* **2011**, *21*, 15167.
(33) Wu, Z.; Li, Y.; Liu, J.; Lu, Z.; Zhang, H.; Yang, B. *Angew. Chem., Int. Ed.* **2014**, *53*, 12196.
(34) Wu, Z.; Dong, C.; Li, Y.; Hao, H.; Zhang, H.; Lu, Z.; Yang, B. *Angew. Chem., Int. Ed.* **2013**, *52*, 9952.
(35) Qing, Z.; He, X.; Qing, T.; Wang, K.; Shi, H.; He, D.; Zou, Z.; Yan, L.; Xu, F.; Ye, X.; Mao, Z. *Anal. Chem.* **2013**, *85*, 12138.
(36) Wu, Z.; Liu, J.; Li, Y.; Cheng, Z.; Li, T.; Zhang, H.; Lu, Z.; Yang, B. *ACS Nano* **2015**, *9*, 6315.

DOI: 10.1021/jacs.5b06550
J. Am. Chem. Soc. 2015, 137, 12906−12913

(37) Benito, Q.; Le Goff, X. F.; Maron, S.; Fargues, A.; Garcia, A.; Martineau, C.; Taulelle, F.; Kahlal, S.; Gacoin, T.; Boilot, J. P.; Perruchas, S. *J. Am. Chem. Soc.* **2014**, *136*, 11311.
(38) Yam, V. W. W.; Cheng, E. C. C.; Zhou, Z. Y. *Angew. Chem., Int. Ed.* **2000**, *39*, 1683.
(39) Yam, V. W. W.; Cheng, E. C. C.; Cheung, K. K. *Angew. Chem., Int. Ed.* **1999**, *38*, 197.
(40) Mei, J.; Hong, Y.; Lam, J. W. Y.; Qin, A.; Tang, Y.; Tang, B. Z. *Adv. Mater.* **2014**, *26*, 5429.
(41) Duan, P.; Yanai, N.; Kurashige, Y.; Kimizuka, N. *Angew. Chem., Int. Ed.* **2015**, *54*, 7544.
(42) Yuan, Y.; Zhang, C. J.; Gao, M.; Zhang, R.; Tang, B. Z.; Liu, B. *Angew. Chem., Int. Ed.* **2015**, *54*, 1780.
(43) Forward, J. M.; Bohmann, D.; Fackler, J. P.; Staples, R. *Inorg. Chem.* **1995**, *34*, 6330.
(44) Nagura, K.; Saito, S.; Yusa, H.; Yamawaki, H.; Fujihisa, H.; Sato, H.; Shimoikeda, Y.; Yamaguchi, S. *J. Am. Chem. Soc.* **2013**, *135*, 10322.
(45) Yuan, W. Z.; Tan, Y.; Gong, Y.; Lu, P.; Lam, J. W. Y.; Shen, X. Y.; Feng, C.; Sung, H. H. Y.; Lu, Y.; Williams, I. D.; Sun, J. Z.; Zhang, Y.; Tang, B. Z. *Adv. Mater.* **2013**, *25*, 2837.
(46) Kim, J. H.; An, B. K.; Yoon, S. J.; Park, S. K.; Kwon, J. E.; Lim, C. K.; Park, S. Y. *Adv. Funct. Mater.* **2014**, *24*, 2745.
(47) Sagara, Y.; Kato, T. *Angew. Chem., Int. Ed.* **2011**, *50*, 9128.
(48) Ma, Z.; Teng, M.; Wang, Z.; Yang, S.; Jia, X. *Angew. Chem., Int. Ed.* **2013**, *52*, 12268.
(49) Sagara, Y.; Komatsu, T.; Ueno, T.; Hanaoka, K.; Kato, T.; Nagano, T. *Adv. Funct. Mater.* **2013**, *23*, 5277.
(50) Balch, A. L. *Angew. Chem., Int. Ed.* **2009**, *48*, 2641.
(51) Krikorian, M.; Liu, S.; Swager, T. M. *J. Am. Chem. Soc.* **2014**, *136*, 2952.
(52) Wang, L.; Zhu, S. J.; Wang, H. Y.; Wang, Y. F.; Hao, Y. W.; Zhang, J.-H.; Chen, Q. D.; Zhang, Y. L.; Han, W.; Yang, B.; Sun, H. *Adv. Opt. Mater.* **2013**, *1*, 264.
(53) Hofbeck, T.; Monkowius, U.; Yersin, H. *J. Am. Chem. Soc.* **2015**, *137*, 399.

DOI: 10.1021/jacs.5b06550
J. Am. Chem. Soc. 2015, 137, 12906−12913